

Beyond BatchNorm: Towards a Unified Understanding of Normalization in Deep Learning

Ekdeep Singh Lubana^{1*}, Robert P. Dick¹, Hidenori Tanaka^{2,3}

¹EECS Department, University of Michigan

²Department of Applied Physics, Stanford University

³Physics & Informatics Laboratories, NTT Research, Inc.

Abstract

Inspired by BatchNorm, there has been an explosion of normalization layers in deep learning. Recent works have identified a multitude of beneficial properties in BatchNorm to explain its success. However, given the pursuit of alternative normalization layers, these properties need to be generalized so that any given layer’s success/failure can be accurately predicted. In this work, we take a first step towards this goal by extending known properties of BatchNorm in randomly initialized deep neural networks (DNNs) to several recently proposed normalization layers. Our primary findings follow: (i) similar to BatchNorm, activations-based normalization layers can prevent exponential growth of activations in ResNets, but parametric techniques require explicit remedies; (ii) use of GroupNorm can ensure an informative forward propagation, with different samples being assigned dissimilar activations, but increasing group size results in increasingly indistinguishable activations for different samples, explaining slow convergence speed in models with LayerNorm; and (iii) small group sizes result in large gradient norm in earlier layers, hence explaining training instability issues in Instance Normalization and illustrating a speed-stability tradeoff in GroupNorm. Overall, our analysis reveals a unified set of mechanisms that underpin the success of normalization methods in deep learning, providing us with a compass to systematically explore the vast design space of DNN normalization layers.

1 Introduction

Normalization techniques are often necessary to effectively train deep neural networks (DNNs) [1, 2, 3]. Arguably, the most popular of these is BatchNorm [1], whose success can be attributed to several beneficial properties that allow it to stabilize a DNN’s training dynamics: for example, ability to propagate informative activation patterns in deeper layers [4, 5]; reduced dependence on initialization [6, 7, 8]; faster convergence via removal of outlier eigenvalues [9, 10]; auto-tuning of learning rates [11], equivalent to modern adaptive optimizers [12]; and smoothing of loss landscape [13, 14]. However, depending on the application scenario, BatchNorm’s use can be of limited benefit or even a hindrance: for example, BatchNorm struggles when training with small batch-sizes [3, 15]; in settings with train-test distribution shifts, BatchNorm can undermine a model’s accuracy [16, 17]; in meta-learning, it can lead to transductive inference [18]; and in adversarial training, it can hamper accuracy on both clean and adversarial examples by estimating incorrect statistics [19, 20].

To either address specific shortcomings or to replace BatchNorm in general, several recent works propose alternative normalization layers (interchangeably called normalizers in this paper). For example, Brock et al. [23] propose to match BatchNorm’s forward propagation behavior in Residual

Email: {eslubana, dickrp}@umich.edu, and hidenori.tanaka@ntt-research.com

*Work partially performed during an internship at Physics & Informatics Laboratories, NTT Research.

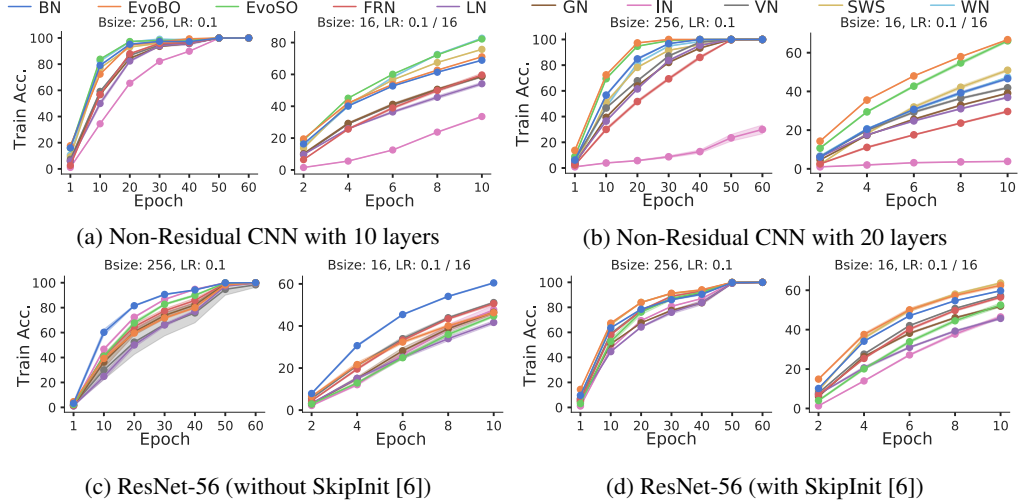


Figure 1: **Each normalization method has its own success and failure modes.** We plot training curves (3 seeds) for different combinations of *normalizer* (see Table 1), *network architecture*, and *batch-size* at largest stable initial learning rate on CIFAR-100. Learning rate is scaled linearly with batch-size [21]. Layers for which loss reaches infinity are not plotted. Test curves and several other settings are provided in the appendix. The plots show that all methods, including BatchNorm (BN), have their respective success and failure modes: e.g., LayerNorm (LN) [2] often converges slowly and Instance Normalization (IN) [22] can have unstable training with large depth or small batch-sizes.

networks [24] by replacing it with Scaled Weight Standardization [25, 26]. Wu and He [3] design GroupNorm, a batch-independent method that groups multiple channels in a layer to perform normalization. Liu et al. [27] use an evolutionary algorithm to search for both normalizers and activation layers. Given the right training configuration, these works show their proposed normalizers often achieve similar test accuracy to BatchNorm and even outperform it on some benchmarks. This begs the question, are we ready to replace BatchNorm? To probe this question, we plot training curves for models defined using different combinations of *normalizer*, *network architecture*, *batch size*, and *learning rate* on CIFAR-100. As shown in Figure 1, clear trends begin to emerge. For example, we see LayerNorm [2] often converges at a relatively slower speed; Weight Normalization [28] cannot be trained at all for ResNets (with and without SkipInit [6]); Instance Normalization [22] results in unstable training in deeper non-residual networks, especially with small batch-sizes. Overall, evaluating hundreds of models in different settings, we see evident success/failure modes exist for all normalization techniques, including BatchNorm.

As we noted before, prior works have established several properties to help explain such success/failure modes for the specific case of BatchNorm. However, given the pursuit of alternative normalizers in recent works, these properties need to be generalized so that one can accurately determine how normalization techniques beyond BatchNorm affect DNN training. In this work, we take a first step towards this goal by extending known properties of BatchNorm *at initialization* to several alternative normalization techniques. As we show, these properties are highly predictive of a normalizer’s influence on DNN training and can help ascertain exactly when an alternative technique is capable of serving as a replacement for BatchNorm. Our contributions follow.

- **Stable Forward Propagation:** In Section 3, we show activations-based normalizers are provably able to prevent exploding variance of activations in ResNets, similar to BatchNorm [5, 6]. Parametric normalizers like Weight Normalization [28] do not share this property; however, we explain why architectural modifications proposed in recent works [6, 7] can resolve this limitation.
- **Informative Forward Propagation:** In Section 4, we first show the ability of a normalizer to generate dissimilar activations for different inputs is a strong predictor of optimization speed. We then extend a known result for BatchNorm to demonstrate the rank of representations in the deepest layer of a Group-normalized [3] model is at least $\Omega(\sqrt{\text{width}/\text{Group Size}})$. This helps us illustrate how use of GroupNorm can prevent high similarity of activations for different inputs if the group size is small, i.e., the number of groups is large. This suggests Instance Normalization [22] (viz.,

GroupNorm with group size equal to 1) is most likely and LayerNorm [2] (viz., GroupNorm with group size equal to layer width) is least likely to produce informative activations.

- **Stable Backward Propagation:** In Section 5, we show normalization techniques that rely on individual sample and/or channel statistics (e.g., Instance Normalization [22]) suffer from an exacerbated case of gradient explosion [29], often witnessing unstable backward propagation. We show this behavior is mitigated by grouping of channels in GroupNorm, thus demonstrating a speed–stability trade-off characterized by group size.

Related Work: Due to its ubiquity, past work has generally focused on understanding BatchNorm [5, 4, 6, 9, 10, 7, 13, 29, 30, 31]. A few works have studied LayerNorm [32, 33], due to its relevance in natural language processing. In contrast, we try to analyze normalization methods in deep learning in a general manner. As we show, we can identify properties in BatchNorm that readily generalize to other normalizers and are often predictive of the normalizer’s impact on training. Our analysis is inspired by a rich body of work focused on understanding randomly initialized DNNs [34, 35, 36, 37, 38]. Most related to us is the contemporary work by Labatie et al. [39], who analyze the impact of different normalization layers on expressivity of activations and conclude LayerNorm leads to high similarity of activations in deeper layers. As we discuss, this result is in fact a special case of our Claim 3.

2 Preliminaries: Normalization Layers for DNNs

We first clarify the notations and operations used by the normalizers discussed in this work. Specifically, we define operators $\mu_{\{d\}}(\mathcal{T})$ and $\sigma_{\{d\}}(\mathcal{T})$, which calculate the mean and standard deviation of a tensor \mathcal{T} along the dimensions specified by set $\{d\}$. $\|\mathcal{T}\|$ denotes the ℓ_2 norm of \mathcal{T} . $\text{RMS}_{\{d\}}(\mathcal{T})$ denotes the root mean square of \mathcal{T} along dimensions specified by set $\{d\}$. For example, for a vector $\mathbf{v} \in \mathbb{R}^n$, we have $\text{RMS}_{\{1\}}(\mathbf{v}) = \sqrt{\sum_i v_i^2/n}$. We assume the outputs of these operators broadcast as per requirements. $\rho(\cdot)$ denotes the sigmoid function. We define symbols b, c, x to denote the batch, channel, and spatial dimensions. For feature maps in a CNN, x will include both the height and the width dimensions. The notation c/g denotes division of c neurons (or channels) into groups of size g . When grouping is performed, each group is normalized independently.

Normalization Layers: We analyze ten normalization layers in this work. These layers were chosen to cover a broad range of ideas: e.g., activations-based layers [1, 40], parametric layers [23, 28], hand-engineered layers [3], AutoML designed layers [27], and layers [22, 2, 4] that form building blocks of recent techniques [41].

1. *Activations-Based Layers:* BatchNorm (BN) [1], LayerNorm (LN) [2], Instance Normalization (IN) [22], GroupNorm (GN) [3], Filter Response Normalization (FRN) [40], Variance Normalization (VN) [4], EvoNormBO [27], and EvoNoRMSO [27] fall in this category. These layers function in the activation space. Note that Variance Normalization is an ablation of BatchNorm that does not use the mean-centering operation. Typically, given activations \mathcal{A}_L at layer L , these layers use an operation of the form $\mathcal{A}_{\text{norm}} = \phi\left(\frac{\gamma}{\sigma_{\{d\}}(\mathcal{A}_L)}(\mathcal{A}_L - \mu_{\{d\}}(\mathcal{A}_L)) + \beta\right)$. Here, γ and β are learned affine parameters used for controlling quantities affected by the normalization operations (such as mean, standard deviation, and RMS) and ϕ is a non-linearity, such as ReLU. The exact operations for these layers, minus the affine parameters, are shown in Table 1.

2. *Parametric Layers:* Weight Normalization (WN) [28] and Scaled Weight Standardization (SWS) [23] fall in this category. Table 1 shows the exact operations. These layers function in the parameter space and act on a filter’s weights (\mathcal{W}) to generate normalized weights ($\mathcal{W}_{\text{norm}}$). The normalized weights $\mathcal{W}_{\text{norm}}$ are used for processing the input: $\mathcal{A}_{L+1} = \phi(\mathcal{W}_{\text{norm}} * \mathcal{A}_L)$.

Activations-Based Layers	
$\mu_{\{d\}} = \mu_{\{d\}}(\mathcal{A}); \sigma_{\{d\}} = \sigma_{\{d\}}(\mathcal{A})$	
BN [1]	$\frac{\mathcal{A} - \mu_{\{b,x\}}}{\sigma_{\{b,x\}}}$
LN [2]	$\frac{\mathcal{A} - \mu_{\{c,x\}}}{\sigma_{\{c,x\}}}$
IN [22]	$\frac{\mathcal{A} - \mu_{\{x\}}}{\sigma_{\{x\}}}$
GN [3]	$\frac{\mathcal{A} - \mu_{\{c/g,x\}}}{\sigma_{\{c/g,x\}}}$
FRN [40]	$\frac{\mathcal{A}}{\text{RMS}_{\{x\}}}$
VN [4]	$\frac{\mathcal{A}}{\sigma_{\{b,x\}}}$
EvoBO [27]	$\frac{\mathcal{A}}{\max\{\sigma_{\{b,x\}}, v \odot \mathcal{A} + \sigma_{\{x\}}\}}$
EvoSO [27]	$\frac{\mathcal{A} \rho(v \odot \mathcal{A})}{\sigma_{\{c/g,x\}}}$
Parametric Layers	
$\mu_{\{d\}} = \mu_{\{d\}}(\mathcal{W}); \sigma_{\{d\}} = \sigma_{\{d\}}(\mathcal{W})$	
WN [28]	$g \frac{\mathcal{W}}{\ \mathcal{W}\ }$
SWS [23]	$g \frac{\mathcal{W} - \mu_{\{c,h,w\}}}{\sigma_{\{c,x\}}}$

Table 1: **Operations performed by different normalizers.** \mathcal{A} denotes layer input; \mathcal{W} denotes incoming neuron weights to a neuron.

3 Stable Forward Propagation

Stable forward propagation is a necessary condition for successful DNN training [36]. In this section, we identify and demystify the role of normalization layers in preventing the problem of *exploding* or *vanishing activations* during forward propagation. These problems can result in training instability due to exploding or vanishing gradients during backward propagation [36, 38]. Building on a previous study on BatchNorm, we first show that activations-based normalizers provably avoid exponential growth of variance in ResNets¹, ensuring training stability. Thereafter, we show parametric normalizers do not share this property and ensuring stable training requires explicit remedies.

3.1 Activations-Based Normalizers and Exponential Variance in Residual Networks

Hanin and Rolnick [38] show that for stable forward propagation in ResNets, the average variance of activations should not grow exponentially (i.e., should not explode). Interestingly, Figure 1 shows that all activations-based normalizers are able to train the standard ResNet [24] architecture stably. For BatchNorm, this behavior is provably expected. Specifically, De and Smith [6] find that to ensure variance along the batch-dimension is 1, BatchNorm rescales the L^{th} layer’s residual path output by a factor of $\mathcal{O}(1/\sqrt{L})$. This causes the growth of variance in a Batch-Normalized ResNet to be linear in depth, hence avoiding exponential growth of variance in and ensuring effective training. We now show this result can be extended to other normalization techniques too.

Claim 1. *Similar to BatchNorm [6], GroupNorm [3] avoids exponential growth of variance in ResNets, ensuring stable training.*

Proof. We follow the same setup as De and Smith [6]. Assume the L^{th} residual path (f_L) is processed by a normalization layer \mathcal{N} , after which it combines with the skip connection to generate the next output: $\mathbf{y}_L = \mathbf{y}_{L-1} + \mathcal{N}(f_L(\mathbf{y}_{L-1}))$. The covariance of layer input and Residual path’s output is assumed to be zero. Hence, the output’s variance is: $\text{Var}(\mathbf{y}_L) = \text{Var}(\mathbf{y}_{L-1}) + \text{Var}(\mathcal{N}(f_L(\mathbf{y}_{L-1})))$. Now, assume GroupNorm with group size G is used for normalizing the D -dimensional activation signal, i.e., $\mathcal{N} = \text{GN}(\cdot)$. This implies for the g^{th} group, $\sigma_{g,x}(\text{GN}(f_L(\mathbf{y}_{L-1}))) = 1$. Then, for a batch of size N , denoting the i^{th} sample activations as $\mathbf{y}_L^{(i)}$, and using $(\mathbf{y}_L^{(i)})^j$ to index the activations, we note the residual output’s variance averaged along the spatial dimension is: $\langle \text{Var}(\mathcal{N}(f_L(\mathbf{y}_{L-1}))) \rangle = \frac{1}{D} \sum_{j=1}^D (\frac{1}{N} \sum_{i=1}^N (\text{GN}(f_L(\mathbf{y}_{L-1})))^j)^2 = \frac{1}{N} \sum_{i=1}^N (\frac{1}{D} \sum_{j=1}^D (\text{GN}(f_L(\mathbf{y}_{L-1})))^{(i)j})^2 = \frac{1}{N} \sum_{i=1}^N \frac{G}{D} (\sum_{g=1}^{D/G} (\sigma_{g,x}(\text{GN}(f_L(\mathbf{y}_{L-1})))^{(i)})^2) = 1$. Overall, this implies $\langle \text{Var}(\mathbf{y}_L) \rangle = \langle \text{Var}(\mathbf{y}_{L-1}) \rangle + 1$. Recursively applying this relationship for a bounded variance input, we see average variance at the L^{th} layer is in $\mathcal{O}(L)$. Thus, similar to BatchNorm, use of GroupNorm will enable stable forward propagation in ResNets by ensuring signal variance grows linearly with depth. \square

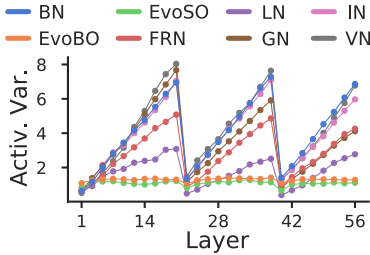


Figure 2: **Activations-based normalizers ensure linear and stable forward propagation, verifying Claim 1.** Activation Variance (Activ. Var.) as a function of layer number in a ResNet-56 [24] processing CIFAR-100 samples.

the remaining layers follow a pattern of linear growth, as expected by our result. We note our

To understand the relevance of the above result, note that for $G = 1$, GroupNorm is equal to Instance Normalization [22] and for $G = D$, GroupNorm is equal to LayerNorm [2]. Further, since the mean of the signal is assumed to be zero, the average variance along the spatial dimension is equal to the RMS_x operation used by Filter Response Normalization [40]. Thus, by proving the above result for GroupNorm, we are able to show alternative activations-based normalizers listed in Table 1 also avoid the exponential growth of activation variance in ResNets.

We show empirical demonstrations of Claim 1 in Figure 2, where the average activation variance is plotted for a ResNet-56. As can be seen, for all activations-based normalizers, the growth of variance is linear in the number of layers. At the end of a Residual module, which spatially downsamples the signal, the variance plummets. However,

¹The case of *non-residual* networks is discussed in appendix. In brief, most normalizers help avoid exploding/vanishing activations by enforcing unit activation variance in the batch, channel, or spatial dimensions.

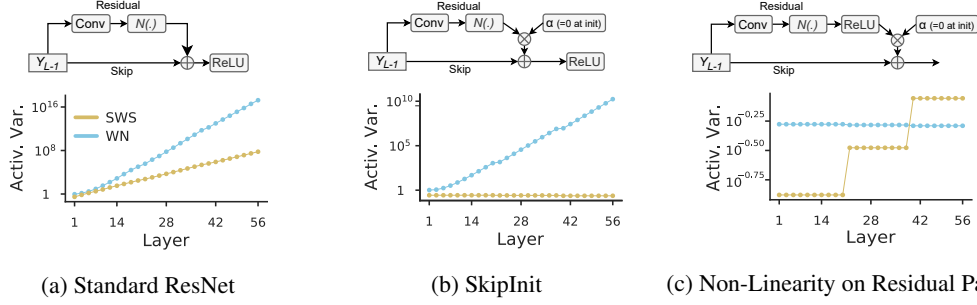


Figure 3: **Parametric normalizers witness exponentially growing variance, verifying Claim 2, but we can stabilize it by modifying the residual-path.** We plot log activation variance as a function of layer number in a randomly initialized ResNet-56 [24], using CIFAR-100 samples, with Scaled Weight Standardization (SWS) [23] and Weight Normalization (WN) [28] for different architectures (simplified illustrations provided on top). (a) *Standard ResNet*: Both SWS and WN witness variance explosion in a standard ResNet model, as claimed in Claim 2. (b) *SkipInit*: SkipInit [6] multiplies the residual signal with a scalar α initialized as zero, thus preventing variance explosion in an SWS model at initialization. Meanwhile, by scaling the non-linearity after addition, a WN model continues to witness exploding variance. (c) *Non-Linearity on Residual Path*: Shifting the non-linearity to the residual path prevents variance explosion in both WN and SWS models.

theory does not apply to EvoNorms, which are designed via AutoML. However, empirically, we see EvoNorms also avoid exponential growth of variance in ResNets. *Thus, our analysis shows, all activations-based normalizers in Table 1 share the beneficial property of stabilizing forward propagation in ResNets, similar to BatchNorm.*

3.2 Parametric Normalizers and Exploding Variance in Residual Networks

By default, parametric normalizers such as Weight Normalization [28] and Scaled Weight Standardization [23] do not preserve the variance of a signal during forward propagation, often witnessing vanishing activations. To address this limitation, properly designed output scale and bias corrections are needed. Specifically, for Weight Normalization and ReLU non-linearity, Arpit et al. [42] show the output should be modified as follows: $\mathcal{A}_{L+1} = \sqrt{2\pi/\pi-1}(\phi(\mathcal{W}_{\text{norm}} * \mathcal{A}_L) - \sqrt{1/2\pi})$. For Scaled Weight Standardization, only output scaling is needed [23]: $\mathcal{A}_{L+1} = \phi(\sqrt{2\pi/\pi-1}\mathcal{W}_{\text{norm}} * \mathcal{A}_L)$.

In Figure 1, ResNet training curves for Weight Normalization [28] and Scaled Weight Standardization [23] were not reported as the loss diverges to infinity. As we explain in the following, this is a result of using correction factors designed to enable variance preservation in non-residual networks.

Claim 2. *Unlike BatchNorm [6], Weight Normalization [28] and Scaled Weight Standardization [23] witness unstable training due to exponential growth of variance in standard ResNets [24].*

Proof. Using the correction factors above, both Weight Normalization and Scaled Weight Standardization will ensure signal variance is preserved on the residual path: $\text{Var}(\mathcal{N}(f(\mathbf{y}_{L-1}))) = \text{Var}(\mathbf{y}_{L-1})$. Thus, using these methods, the output variance at layer L becomes: $\text{Var}(\mathbf{y}_L) = \text{Var}(\mathbf{y}_{L-1}) + \text{Var}(\mathcal{N}(f(\mathbf{y}_{L-1}))) = 2 \text{Var}(\mathbf{y}_{L-1})$. Recursively applying this relationship for a bounded variance input, we see signal variance at the L^{th} layer is in $\mathcal{O}(2^L)$. Thus, Weight Normalization and Scaled Weight Standardization witness exponential growth in variance. \square

More generally, the above result shows if the residual path is variance preserving, ResNets will witness exploding variance with growing depth. Prior works [43, 5, 8, 6, 7, 44] have noted this result in the context of designing effective ResNet initializations. *Here, we extended this result to show why Weight Normalized and Scaled Weight Standardized ResNets undergo unstable forward propagation.* Empirical demonstration is provided in Figure 3a.

In their work introducing Scaled Weight Standardization [23], Brock et al. are able to circumvent exponential growth in variance by using SkipInit [6]. Specifically, inspired by the fact that BatchNorm biases Residual paths to identity functions, De and Smith [6] propose SkipInit, which multiplies the output of the residual path by a learned scalar α that is initialized to zero. This suppresses the Residual path’s contribution, hence avoiding exponential growth in variance (see Figure 3b). Interestingly, even

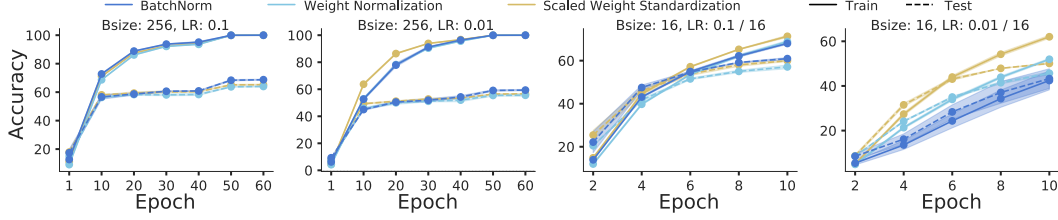


Figure 4: **Modified residual-path allows for successful training with parametric layers.** We plot train/test accuracy (over 3 seeds) for ResNet-56 architecture on CIFAR-100 with non-linearity located on the residual path. We see parametric normalizers can train effectively if scaled non-linearities are not located after the addition operation in a ResNet.

after using SkipInit, we find Weight Normalized ResNets witness variance explosion (see Figure 3b). To explain this behavior, we note that in the standard ResNet architecture, the non-linearity is located after the addition operation of skip connection and the residual path’s signals (see Figure 3a). Thus, even if SkipInit is used to suppress the residual path, the non-linearity will still be applied to the skip connections. Since the scale correction for Weight Normalization ($\sqrt{2\pi/\pi-1}$) is greater than 1, this implies the signal output is amplified at every layer to preserve signal variance; however, since convolutions are absent on the skip path, signal variance never decays. Consequently, *variance is only amplified*, causing the variance to increase exponentially in the number of layers (see Figure 3b).

Training ResNets with Weight Normalization: The above discussion shows that for Weight Normalization, since the output has to be scaled-up to preserve signal variance, standard ResNets [24] witness exploding activations. This also hints at a solution: place the non-linearity on the Residual path. This modification (see Figure 3c) in fact results in one of the architectures proposed by He et al. in their original work on ResNets [45]. We verify the effectiveness of this modification in Figure 3c. As can be seen, the signal variance in a Weight Normalized ResNet stays essentially constant for this architecture. Furthermore, we show in Figure 4 that these models are able to match BatchNorm in performance for several training configurations. In general, our discussion here explains *the exact reasons why architectures with non-linearity on residual path are better suited for parametric normalizers*. Finally, we note that another ResNet architecture which boasts non-linearity on residual paths is pre-activation ResNets [45]. In their experimental setup for designing Scaled Weight Standardization [23], Brock et al. specifically focused on pre-activation ResNets [45]. This is another reason why the problem of exploding activations does not surface in their work.

4 Informative Forward Propagation

Proper magnitude of activations is a necessary, but not sufficient, condition for successful training. Here, we study another failure mode for forward propagation, *rank collapse*, where activations for different input samples become indistinguishably similar in deeper layers. This can significantly slow training as the gradient updates no longer reflect information about the input data [4]. To understand this problem’s relevance, we first show why the ability to generate dissimilar activations is useful in the context of normalization methods for deep learning. Specifically, given a randomly initialized network that uses a specific normalizer, we relate its average cosine similarity of activations at the penultimate layer (i.e., layer before the linear classifier) with its mean training accuracy ($= \frac{\sum_{i=1}^{\# \text{ of epochs}} \text{Train Acc.}[i]}{\# \text{ of epochs}}$, a measure of optimization speed [46]). Results for three different architectures (Non-Residual CNN with 10 layers and 20 layers as well as ResNet-56 without SkipInit) are shown in Figure 5. As can be seen, the correlation between mean training accuracy and the average cosine similarity of activations is high. *In fact, for any given network architecture, one can predict which normalizer will enable the fastest convergence without even training the model.* This shows normalizers which result in more dissimilar representations at initialization are likely to be more useful for training DNNs.

We now note another interesting pattern in Figure 5: *LayerNorm results in highest similarity of activations for any given architecture.* To explain this, we again revisit known properties of BatchNorm. As shown by Daneshmand et al. [4, 47], BatchNorm provably ensures activations generated by a randomly initialized network have high rank, i.e., different samples have sufficiently different activations. To derive this result, the authors consider activations for N samples at the penultimate layer, $Y \in \mathbb{R}^{\text{width} \times N}$, and define the covariance matrix YY^T , whose rank is equal to that of the

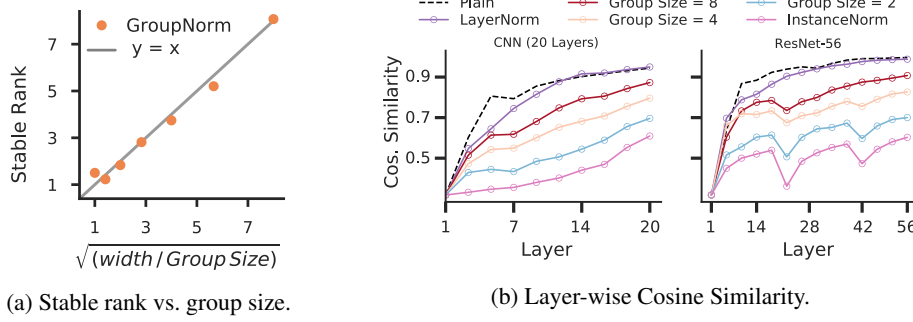


Figure 6: **The smaller the group size, the higher the rank of the activations, verifying Claim 3** (a) We plot stable rank of activations at the penultimate layer for random Gaussian inputs. As proposed in Claim 3, we find a perfect linear fit between stable rank and values of $\sqrt{\text{Width}/\text{Group Size}}$ for different group sizes. (b) Implications of Claim 3 on CIFAR-100 samples: by increasing group size (constant across layers), we see similarity of features at any given layer increases. This shows LayerNorm [2] cannot generate informative features, thus witnessing slow convergence (see Figure 5).

similarity matrix $Y^T Y$. The authors then show that in a zero-mean, randomly initialized network with BatchNorm layers, the covariance matrix will have a rank at least as large as $\Omega(\sqrt{\text{width}})$. That is, there are at least $\Omega(\sqrt{\text{width}})$ distinct directions that form the basis of the similarity matrix, hence indicating the model is capable of extracting informative activations. In the following, we propose a claim that extends this result to activations-based normalizers beyond BatchNorm.

Claim 3. *For a zero-mean, randomly initialized network with GroupNorm [3] layers, the penultimate layer activations have a rank of at least $\Omega(\sqrt{\text{width}/\text{Group Size}})$, where width denotes the layer-width (e.g., number of channels in a CNN).*

The intuition behind the above claim is based on the proof by Daneshmand et al. [4]. In their work, the authors extend a prior result from random matrix theory which suggests multiplication of several zero-mean, randomly initialized gaussian matrices will result in a rank-one matrix [10]. The use of BatchNorm ensures that on multiplication with a randomly initialized weight matrix, the values of on-diagonal elements of the covariance matrix $Y Y^T$ are preserved, while the off-diagonal elements are suppressed. This leads to a lower bound of the order of $\Omega(\sqrt{\text{width}})$ on the stable rank [48] of the covariance matrix. Now, if one directly considers the similarity matrix $Y^T Y$ and uses GroupNorm instead of BatchNorm, then a similar preservation and suppression of on- and off-diagonal *matrix blocks* should occur. Here, the block size will be equal to the Group size used for GroupNorm. This indicates the lower bound is in $\Omega(\sqrt{\text{width}/\text{Group Size}})$.

We provide demonstration of this claim in Figure 6a. We use a similar setup as Daneshmand et al. [4], randomly initializing a CNN with constant layer-width (64) and 30 layers. A GroupNorm layer is placed before every ReLU layer and the group size is swepted from 1 to 64. As seen in Figure 6a, we find a perfect linear fit between the stable rank and the value of $\sqrt{\text{width}/\text{Group Size}}$, validating our claim empirically as well.

To understand the significance of Claim 3, note that the result shows if the group size is large, then use of GroupNorm cannot prevent collapse of representations (i.e., cannot result in informative activations). To demonstrate this effect, we calculate the mean cosine similarity of activations between different samples of a randomly initialized network that uses GroupNorm. We sweep the group size from layer-width to 1, thus covering the spectrum from LayerNorm (Group Size

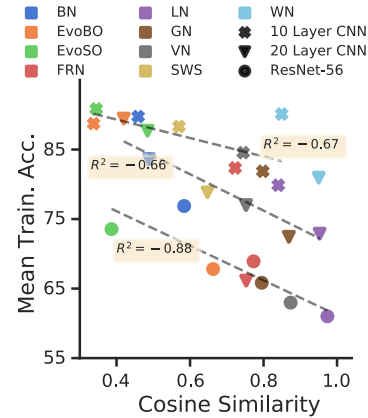


Figure 5: **Informative forward propagation results in faster optimization.** We plot mean training accuracy ($= \frac{\sum_{i=1}^{\# \text{ of epochs}} \text{Train Acc.}[i]}{\# \text{ of epochs}}$) on CIFAR-100 vs. average cosine similarity at initialization. As shown, normalizers which induce dissimilar activations converge faster. Instance Normalization was removed due to training instability (see Section 5).

= layer-width) to Instance Normalization (Group Size = 1). We analyze both a non-residual CNN with 20 layers and a ResNet-56. Results are shown in Figure 6b and confirm our claim that by grouping the entire layer for normalization, LayerNorm results in highly similar activations. *This explains the slow convergence behavior of LayerNorm in Figure 5.* Meanwhile, if we reduce the group size, similarity of representations decreases as well, indicating generation of informative activations. This shows use of GroupNorm with group size greater than layer-width can help prevent a collapse of features onto a single representation. Importantly, this result helps explain why GroupNorm can serve as a successful replacement for BatchNorm in similarity based self-supervised learning frameworks [49], which often witness representation collapse issues [50]. Similar to BatchNorm, GroupNorm helps discriminate between representations of different inputs, helping avoid a collapse of representations.

5 Stable Backward Propagation

Taking the results of Section 4 to the extreme should imply Instance Normalization (i.e., Group Size = 1) is the best configuration for GroupNorm, but as we noted in Figure 1, Instance Normalization witnesses unstable training. To explain this, we describe a “speed-stability” trade-off in GroupNorm in the next section by extending the property of gradient explosion in BatchNorm to alternative normalization layers. Specifically, Yang et al. [29] recently show that gradient norm in earlier layers of a randomly-initialized BatchNorm network increases exponentially with increasing model depth (see Figure 8). This shows the maximum depth of a model trainable with BatchNorm is finite. The theory leading to this result is quite involved, but a much simpler analysis can not only explain this phenomenon accurately, but also illustrate the existence of gradient explosion in alternative layers.

Gradient explosion in BatchNorm: Following Luther [51], we analyze the origin of gradient explosion based on the expression of gradient backpropagated through a BatchNorm layer. We calculate the gradient of loss w.r.t. activations at layer L , denoted as $\mathbf{Y}_L \in \mathbb{R}^{d_L \times N}$. We define two sets of intermediate variables: (i) pre-activations, generated by weight multiplication, $X_L = W_L Y_{L-1}$ and (ii) normalized pre-activations, generated by BatchNorm, $\hat{X}_L = \text{BN}(X_L) = \frac{\gamma}{\sigma_{\{N\}}(X_L)}(X_L - \mu_{\{N\}}(X_L)) + \beta$. Under these notations, the gradient backpropagated from layer L to layer $L-1$ is (see appendix for derivation): $\nabla_{\mathbf{Y}_{L-1}}(J) = \frac{\gamma}{\sigma_{\{N\}}(X_L)} \mathcal{W}_L^T \mathcal{P}[\nabla_{\hat{\mathbf{X}}_L}(J)]$. Here \mathcal{P} is a composition of two projection operators: $\mathcal{P}[\mathbf{Z}] = \mathcal{P}_{\mathbf{1}_N}^\perp [\mathcal{P}_{\text{Ob}(\hat{\mathbf{X}}_L/\sqrt{N})}^\perp [\mathbf{Z}]]$. The operator $\mathcal{P}_{\text{Ob}(\hat{\mathbf{X}}_L/\sqrt{N})}^\perp [\mathbf{Z}] = \mathbf{Z} - \frac{1}{N} \text{diag}(\mathbf{Z} \hat{\mathbf{X}}_L^T) \hat{\mathbf{X}}_L$ subtracts its input’s component that is inline with the BatchNorm outputs via projection onto the Oblique manifold $\text{diag}(\frac{1}{N} \hat{\mathbf{X}}_L \hat{\mathbf{X}}_L^T) = \text{diag}(\mathbf{1})$. Similarly, $\mathcal{P}_{\mathbf{1}_N}^\perp [\mathbf{Z}] = \mathbf{Z}(\mathbf{I} - \frac{1}{N} \mathbf{1}_N \mathbf{1}_N^T)$ mean-centers its input along the batch dimension via projection onto $\mathbf{1}_N \in \mathbb{R}^N$.

Notice that at initialization, the gradient is unlikely to have a large component along specific directions such as the all-ones vector ($\mathbf{1}$) or the oblique manifold defined by $\hat{\mathbf{X}}_L$. Thus, the gradient norm will remain essentially unchanged when propagating through the projection operation (\mathcal{P}). However, the next operation, multiplication with $\frac{\gamma}{\sigma_{\{N\}}(X_L)} (= \frac{1}{\sigma_{\{N\}}(X_L)}$ at initialization) will re-scale the gradient norm according to the standard deviation of pre-activations along the batch dimension. As shown by Luther [51], for a standard, zero-mean Gaussian initialization, the pre-activations have a standard deviation equal to $\sqrt{\pi-1}/\pi < 1$. Thus, at initialization, the division by standard deviation operation *amplifies* the gradient during backward propagation. For each BatchNorm layer in the model, such an amplification of the gradient will take place, hence resulting in an exponential increase in the gradient norm at earlier layers. Overall, our analysis exposes an interesting tradeoff in BatchNorm: *Division by standard deviation during forward propagation, which is important for generating dissimilar activations [4], results in gradient explosion during backward propagation, critically limiting the maximum trainable model depth!* Empirically, the above analysis is quite accurate near initialization. For example, in Figure 7, we show that the correlation between the norm of the gradient at a layer ($\|\nabla_{\mathbf{Y}_L}(J)\|$) and the inverse product of standard deviation of the pre-activations of layers ahead of it ($\prod_{l=10}^{L+1} 1/\sigma_{\{N\}}(\mathbf{x}_l)$) remains very high (0.6–0.9) over the first few hundred iterations in a 10-layer CNN trained on CIFAR-100.

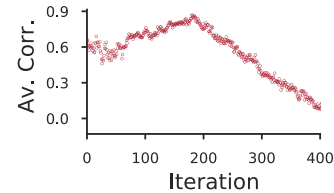


Figure 7: **Gradient norm vs. pre-activation statistics.** We see high correlation between gradient norm and inverse product of layer-wise pre-activation std. deviations.

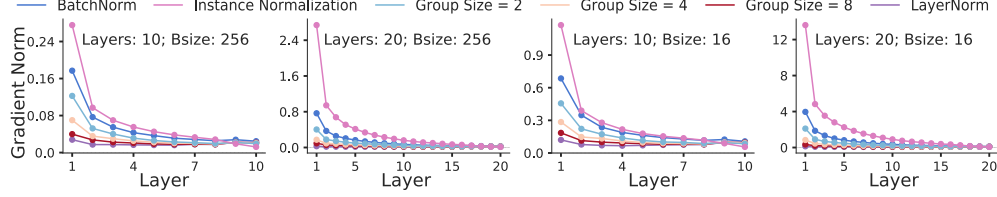


Figure 8: **Small group size increases gradient explosion, verifying Claim 4.** We use CIFAR-100 samples and plot layer-wise gradient norm for different models and batch sizes. As shown, Instance Normalization [22] undergoes highest gradient explosion, followed by BatchNorm [1], GroupNorm [3], and LayerNorm [2] in all settings.

Gradient Explosion in Other Normalizers: We now extend the phenomenon of gradient explosion to other normalizers. The primary idea is that since all activation-based normalizers have a gradient expression similar to BatchNorm (i.e., projection followed by division by standard deviation), they all re-scale the gradient norm during backprop. However, the statistic used for normalization varies across normalizers, resulting in different severity of gradient explosion.

Claim 4. *For a given set of pre-activations, the backpropagated gradient undergoes higher average amplification through an Instance Normalization layer [22] than through a BatchNorm layer [1]. Further, GroupNorm [3] witnesses lesser gradient explosion than both these layers.*

Proof. The gradient backpropagated through the g^{th} group in a GroupNorm layer with group-size G is expressed as: $\nabla_{\mathbf{Y}_{L-1}^g}(J) = \frac{\gamma}{\sigma_{\{g\}}(\mathbf{X}_L^g)} \mathcal{W}_L^T \mathcal{P}[\nabla_{\hat{\mathbf{X}}_L^g}(J)]$ (see appendix for derivation). Here, \mathcal{P} is defined as: $\mathcal{P}[\mathbf{Z}] = \mathcal{P}_1^\perp[\mathcal{P}_{\mathbb{S}(\hat{\mathbf{X}}_L/\sqrt{G})}^\perp[\mathbf{Z}]]$, where $\mathcal{P}_{\mathbb{S}(\hat{\mathbf{X}}_L/\sqrt{G})}^\perp[\mathbf{Z}] = (I - \frac{1}{G} \hat{\mathbf{X}}_L^g \hat{\mathbf{X}}_L^{gT}) \mathbf{Z}$. That is, the component of gradient inline with the normalized pre-activations will be removed via projection onto the spherical manifold defined by $\|\hat{\mathbf{X}}_L^g\| = \sqrt{G}$. As can be seen, the gradient expressions for GroupNorm and BatchNorm are very similar. Hence, the discussion for gradient explosion in BatchNorm directly applies to GroupNorm as well. This implies, when Instance Normalization is used in a CNN, the gradient norm for a given channel c and the i^{th} sample is amplified by the factor $\frac{1}{\sigma_{\{x\}}(\mathbf{X}_{L,i}^c)}$ (inverse of spatial standard deviation). Then, over N samples, using the arithmetic-mean \geq harmonic-mean inequality, we see the average gradient amplification in Instance Normalization is greater than gradient amplification in BatchNorm: $\frac{1}{N} \sum_i \frac{1}{\sigma_{\{x\}}^2(\mathbf{X}_{L,i}^c)} \geq \frac{N}{\sum_i \sigma_{\{x\}}^2(\mathbf{X}_{L,i}^c)} = \frac{1}{\sigma_{\{N\}}^2(\mathbf{X}_L)}$.

Similarly applying arithmetic-mean \geq harmonic-mean for a given sample and the g^{th} group, we see average gradient amplification in Instance Normalization is greater than gradient amplification in GroupNorm: $\frac{1}{G} \sum_c \frac{1}{\sigma_{\{x\}}^2(\mathbf{X}_{L,i}^{g,c})} \geq \frac{G}{\sum_c \sigma_{\{x\}}^2(\mathbf{X}_{L,i}^{g,c})} = \frac{1}{\sigma_{\{g\}}^2(\mathbf{X}_L)}$. Extending this last inequality by averaging over N samples, we see average gradient amplification in GroupNorm is lower than that in BatchNorm. *This implies grouping of neurons in GroupNorm helps reduce gradient explosion.* \square

We show empirical verification of Claim 4 in Figure 8. As can be seen, the gradient norm in earlier layers follows the order Instance Normalization \geq BatchNorm \geq GroupNorm \geq LayerNorm, as proved in Claim 4. Further, since increasing depth implies more normalization operations, we see gradient explosion increases as depth increases. Similarly, since reducing batch-size increases gradient noise, we find gradient explosion increases with decrease in batch-size as well.

Speed-stability trade-off in GroupNorm: Combined with Section 4, our discussion in this section helps identify a speed-stability trade-off in GroupNorm. Specifically, we find that while GroupNorm with group size equal to 1 (viz., Instance Normalization) results in more diverse features (see Claim 3), it is also more susceptible to gradient explosion and hence sees training instability for small batch-sizes/large model depth (see Figure 1). Meanwhile, when group size is equal to layer-width (viz., LayerNorm), gradient explosion can be avoided, but the model is unable to generate informative activations and thus witnesses slower optimization. Combining these

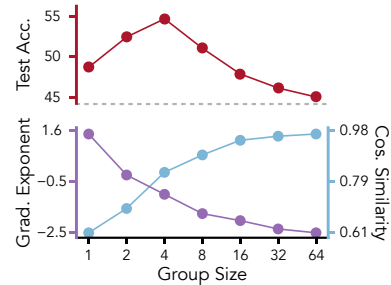


Figure 9: **Speed-Stability trade-off in GroupNorm** using 20-layer CNNs with batch-size 256 on CIFAR-100. We see increasing group size decreases gradient explosion (improved training stability) at the expense of high activation similarity (reduced optimization speed).

results demonstrates that the group size in GroupNorm ensues a trade-off between high similarity of activations (influences training speed) and gradient explosion (influences training stability). To illustrate this trade-off, we can estimate training instability by fitting an exponential curve to layerwise gradient norms (measures degree of gradient explosion) and estimate training speed by calculating cosine similarity of activations at the penultimate layer at initialization (highly correlated with training speed; see Figure 6). Results are shown in Figure 9. We see increasing group size clearly trades-off the two properties related to training speed and stability, with a moderately large group size resulting in best performance. In fact, we see test accuracy is highest exactly at this point of intersection in the trade-off. This explains the success of channel grouping in GroupNorm and other successful batch-independent normalization layers like EvoNormSO [27]. Interestingly, these results also help explain why in comparison to BatchNorm, which suffers from gradient explosion and exacerbates the problem of high gradient variance in non-IID Federated learning setups [52, 53], use of GroupNorm with a properly tuned group-size helps achieve better performance [52, 54].

6 Discussion and Limitations

Discussion: As the number of deep learning architectures continues to explode, the use of normalization layers is becoming increasingly common. However, past works provide minimal insight into what makes normalization layers beyond BatchNorm (un)successful. Our work acts as a starting point to bridge this gap. Specifically, we extend known results on benefits/limitations of BatchNorm to recently proposed normalization layers and provide a thorough characterization of their behavior at initialization. This generalized analysis provides a compass that can help systematically infer which normalization layer is most appealing under the constraints imposed by a given application, reducing reliance on empirical benchmarking. Moreover, since our results show phenomenon used to explain BatchNorm’s success exist in alternative normalizers as well, we argue the success of BatchNorm requires further characterization. Our work also opens avenues for several new fronts of research. For example, in Section 4 we demonstrated that a normalization layer’s impact on similarity of activations accurately predicts resulting optimization speed. As shown in a contemporary work by Boopathy and Fiete [55], the weight update dynamics of a neural network are in fact guided by the matrix defining similarity of activations. Beyond providing grounding to our observation, their results indicate that relating design choices in neural network development with similarity of activations can help optimize their values. Indeed, a recent method for neural architecture search directly utilizes the similarity of activations to design “good” architectures [56].

Limitations: In this work, we limit our focus to discriminative vision applications. We highlight that nine out of ten normalizers studied in this work were specifically designed for this setting and we indeed find that all our analyzed properties show predictive control over the final performance of a model in discriminative vision tasks, generalizing across multiple network architectures. However, extending our work to develop similar analyses in other contexts such as NLP will be very useful. The primary hurdle is that for different data modalities, the standard architecture families and their corresponding optimization difficulties vary widely. For example, in both LSTM and transformer architectures, an often noted training difficulty arises from large gradient norms, which can result in divergent training or training restarts [57, 58]. In fact, optimizers in existing NLP frameworks have gradient clipping enabled by default to avoid this problem [59]. Beyond large gradients, unbalanced gradients are also known to be a training difficulty in NLP architectures [60]. We think a thorough treatment of the role of normalization layers in addressing these problems will be very valuable and leave it for future work.

Acknowledgements

We thank Hadi Daneshmand and anonymous reviewers for several helpful discussions that helped improve this paper. This work was partly supported by NSF under award CNS-2008151.

References

- [1] Sergey Ioffe and Christian Szegedy. Batch Normalization: Accelerating Deep Network Training by Reducing Internal Covariate Shift. In *Proc. Int. Conf. on Machine Learning (ICML)*, Jul 2015.

- [2] Jimmy Lei Ba, Jamie Ryan Kiros, and Geoffrey E. Hinton. Layer Normalization. *arXiv*, abs/1607.08022, 2016.
- [3] Yuxin Wu and Kaiming He. Group Normalization. In *Proc. European Conf. on Computer Vision (ECCV)*, 2018.
- [4] Hadi Daneshmand, Jonas Kohler, Francis Bach, Thomas Hofmann, and Aurelien Lucchi. Batch normalization provably avoids ranks collapse for randomly initialised deep networks. In *Proc. Adv. in Neural Information Processing Systems (NeurIPS)*, 2020.
- [5] David Balduzzi, Marcus Frean, Lennox Leary, J. P. Lewis, Kurt Wan-Duo Ma, and Brian McWilliams. The Shattered Gradients Problem: If resnets are the answer, then what is the question? In *Proc. Int. Conf. on Machine Learning (ICML)*, Aug 2017.
- [6] Soham De and Samuel L. Smith. Batch Normalization Biases Residual Blocks Towards the Identity Function in Deep Networks. In *Proc. Adv. in Neural Information Processing Systems (NeurIPS)*, 2020.
- [7] Jie Shao, Kai Hu, Changhu Wang, Xiangyang Xue, and Bhiksha Raj. Is normalization indispensable for training deep neural network? In *Proc. Adv. in Neural Information Processing Systems (NeurIPS)*, 2020.
- [8] Hongyi Zhang, Yann N. Dauphin, and Tengyu Ma. Residual Learning Without Normalization via Better Initialization. In *Proc. Int. Conf. on Learning Representations (ICLR)*, 2019.
- [9] Ryo Karakida, Shotaro Akaho, and Shun-ichi Amari. The normalization method for alleviating pathological sharpness in wide neural networks. In *Proc. Adv. in Neural Information Processing Systems (NeurIPS)*, 2019.
- [10] Nils Bjorck, Carla P Gomes, Bart Selman, and Kilian Q Weinberger. Understanding Batch Normalization. In *Proc. Adv. in Neural Information Processing Systems (NeurIPS)*, 2018.
- [11] Sanjeev Arora, Zhiyuan Li, and Kaifeng Lyu. Theoretical Analysis of Auto Rate-Tuning by Batch Normalization. In *Proc. Int. Conf. on Learning Representations (ICLR)*, 2019.
- [12] Hidenori Tanaka and Daniel Kunin. Noether’s Learning Dynamics: The Role of Kinetic Symmetry Breaking in Deep Learning. *arXiv preprint arXiv:2105.02716*, 2021.
- [13] Shibani Santurkar, Dimitris Tsipras, Andrew Ilyas, and Aleksander Mądry. How Does Batch Normalization Help Optimization? In *Proc. Adv. in Neural Information Processing Systems (NeurIPS)*, 2018.
- [14] Hongwei Yong, Jianqiang Huang, Xiansheng Hua, and Lei Zhang. Gradient Centralization: A New Optimization Technique for Deep Neural Networks. In *Proc. European Conf. on Computer Vision (ECCV)*, 2020.
- [15] Sergey Ioffe. Batch Renormalization: Towards Reducing Minibatch Dependence in Batch-Normalized Models. In *Proc. Adv. in Neural Information Processing Systems (NeurIPS)*, 2017.
- [16] Cecilia Summers and Michael J. Dinneen. Four Things Everyone Should Know to Improve Batch Normalization. In *Proc. Int. Conf. on Learning Representations (ICLR)*, 2020.
- [17] Ximei Wang, Ying Jin, Mingsheng Long, Jianmin Wang, and Michael I. Jordan. Transferable Normalization: Towards Improving Transferability of Deep Neural Networks. In *Proc. Adv. in Neural Information Processing Systems (NeurIPS)*, 2020.
- [18] John Bronskill, Jonathan Gordon, James Requeima, Sebastian Nowozin, and Richard E. Turner. TaskNorm: Rethinking Batch Normalization for Meta-Learning. In *Proc. Int. Conf. on Machine Learning (ICML)*, Jul 2020.
- [19] Angus Galloway, Anna Golubeva, Thomas Tanay, Medhat Moussa, and Graham W. Taylor. Batch Normalization is a Cause of Adversarial Vulnerability. *arXiv*, abs/1905.02161, 2019.

- [20] Cihang Xie, Mingxing Tan, Boqing Gong, Jiang Wang, Alan L. Yuille, and Quoc V. Le. Adversarial Examples Improve Image Recognition. In *Proc. Int. Conf. on Computer Vision and Pattern Recognition (CVPR)*, 2020.
- [21] Priya Goyal, Piotr Dollár, Ross Girshick, Pieter Noordhuis, Lukasz Wesolowski, Aapo Kyrola, Andrew Tulloch, Yangqing Jia, and Kaiming He. Accurate, Large Minibatch SGD: Training ImageNet in 1 Hour. In *Proc. Int. Conf. on Computer Vision and Pattern Recognition (CVPR)*, 2018.
- [22] Dmitry Ulyanov, Andrea Vedaldi, and Victor S. Lempitsky. Instance Normalization: The Missing Ingredient for Fast Stylization. *arXiv*, abs/1607.08022, 2016.
- [23] Andrew Brock, Soham De, and Samuel L Smith. Characterizing signal propagation to close the performance gap in unnormalized ResNets. In *Proc. Int. Conf. on Learning Representations (ICLR)*, 2021.
- [24] Kaiming He, Xiangyu Zhang, Shaoqing Ren, and Jian Sun. Deep Residual Learning for Image Recognition. In *Proc. Int. Conf. on Computer Vision and Pattern Recognition (CVPR)*, 2016.
- [25] Siyuan Qiao, Huiyu Wang, Chenxi Liu, Wei Shen, and Alan Yuille. Micro-Batch Training with Batch-Channel Normalization and Weight Standardization. *arXiv*, abs/1903.10520, 2019.
- [26] Lei Huang, Xianglong Liu, Yang Liu, Bo Lang, and Dacheng Tao. Centered Weight Normalization in Accelerating Training of Deep Neural Networks. In *Proc. Int. Conference on Computer Vision (ICCV)*, 2017.
- [27] Hanxiao Liu, Andrew Brock, Karen Simonyan, and Quoc V. Le. Evolving Normalization-Activation Layers. In *Proc. Adv. in Neural Information Processing Systems (NeurIPS)*, 2020.
- [28] Tim Salimans and Diederik P. Kingma. Weight Normalization: A Simple Reparameterization to Accelerate Training of Deep Neural Networks. In *Proc. Int. Conf. on Learning Representations (ICLR)*, 2016.
- [29] Greg Yang, Jeffrey Pennington, Vinay Rao, Jascha Sohl-Dickstein, and Samuel S. Schoenholz. A Mean Field Theory of Batch Normalization. In *Int. Conf. on Learning Representations (ICLR)*, 2019.
- [30] Yuxin Wu and Justin Johnson. Rethinking “Batch” in BatchNorm. *arXiv preprint arXiv:2105.07576*, 2021.
- [31] Vinay Rao and Jascha Sohl-Dickstein. Is Batch Norm unique? An empirical investigation and prescription to emulate the best properties of common normalizers without batch dependence. *arXiv*, abs/2010.10687, 2020.
- [32] Jingjing Xu, Xu Sun, Zhiyuan Zhang, Guangxiang Zhao, and Junyang Lin. Understanding and Improving Layer Normalization. In *Proc. Adv. in Neural Information Processing Systems (NeurIPS)*, 2019.
- [33] Sheng Shen, Zhewei Yao, Amir Gholami, Michael Mahoney, and Kurt Keutzer. Powernorm: Rethinking batch normalization in transformers. In *ICML*, 2020.
- [34] Xavier Glorot and Yoshua Bengio. Understanding the difficulty of training deep feedforward neural networks. In *Proc. Int. Conf. on Artificial Intelligence and Statistics (AISTATS)*, 2010.
- [35] Jeffrey Pennington, Samuel S. Schoenholz, and Surya Ganguli. Resurrecting the sigmoid in deep learning through dynamical isometry: theory and practice. In *Proc. Adv. in Neural Information Processing Systems (NeurIPS)*, 2017.
- [36] Samuel S. Schoenholz, Justin Gilmer, Surya Ganguli, and Jascha Sohl-Dickstein. Deep Information Propagation. In *Proc. Int. Conf. on Learning Representations (ICLR)*, 2017.
- [37] Antoine Labatie. Characterizing Well-Behaved vs. Pathological Deep Neural Networks. In *Proc. Int. Conf. on Machine Learning (ICML)*, Jul 2019.

- [38] Boris Hanin and David Rolnick. How to Start Training: The Effect of Initialization and Architecture. In *Proc. Adv. in Neural Information Processing Systems (NeurIPS)*, 2018.
- [39] Antoine Labatie, Dominic Masters, Zach Eaton-Rosen, and Carlo Luschi. Proxy-Normalizing Activations to Match Batch Normalization while Removing Batch Dependence. *arXiv preprint arXiv:2106.03743*, 2021.
- [40] Saurabh Singh and Shankar Krishnan. Filter Response Normalization Layer: Eliminating Batch Dependence in the Training of Deep Neural Networks. In *Proc. Int. Conf. on Computer Vision and Pattern Recognition (CVPR)*, 2019.
- [41] Ping Luo, Peng Zhanglin, Shao Wenqi, Zhang Ruimao, Ren Jiamin, and Wu Lingyun. Differentiable Dynamic Normalization for Learning Deep Representation. In *Proc. Int. Conf. on Machine Learning (ICML)*, June 2019.
- [42] Devansh Arpit, Yingbo Zhou, Bhargava Kota, and Venu Govindaraju. Normalization Propagation: A Parametric Technique for Removing Internal Covariate Shift in Deep Networks. In *Proc. Int. Conf. on Machine Learning (ICML)*, Jul 2016.
- [43] Masato Taki. Deep Residual Networks and Weight Initialization. *arXiv*, abs/1709.02956, 2017.
- [44] Haozhi Qi, Chong You, Xiaolong Wang, Yi Ma, and Jitendra Malik. Deep Isometric Learning for Visual Recognition. In *Proc. Int. Conf. on Machine Learning (ICML)*, Jul 2020.
- [45] Kaiming He, Xiangyu Zhang, Shaoqing Ren, and Jian Sun. Identity Mappings in Deep Residual Networks. In *Proc. European Conf. on Computer Vision (ECCV)*, 2016.
- [46] Behnam Neyshabur, Hanie Sedghi, and Chiyuan Zhang. What is being transferred in transfer learning? In *Proc. Adv. in Neural Information Processing Systems (NeurIPS)*, 2020.
- [47] Hadi Daneshmand, Amir Joudaki, and Francis Bach. Batch Normalization Orthogonalizes Representations in Deep Random Networks. *arXiv preprint arXiv:2106.03970*, 2021.
- [48] Joel A. Tropp. An Introduction to Matrix Concentration Inequalities. *arXiv*, abs/1501.01571, 2015.
- [49] Pierre Richemond, Jean-Bastien Grill, Florent Altché, Corentin Tallec, Florian Strub, Andrew Brock, Samuel Smith, Soham De, Razvan Pascanu, Bilal Piot, and Michal Valko. BYOL works even without batch statistics. *arXiv preprint arXiv:2010.10241*, 2020.
- [50] Xinlei Chen and Kaiming He. Exploring Simple Siamese Representation Learning. *arXiv preprint arXiv:2011.10566*, 2020.
- [51] Kyle Luther. Why Batch Norm Causes Exploding Gradients. <https://kyleluther.github.io/2020/02/18/batchnorm-exploding-gradients.html>, 2020. Blogpost.
- [52] Zhengming Zhang, Yaoqing Yang, Zhewei Yao, Yujun Yan, Joseph Gonzalez, and Michael Mahoney. Improving Semi-supervised Federated Learning by Reducing the Gradient Diversity of Models. *arXiv preprint arXiv:2008.11364*, 2020.
- [53] Jianyu Wang, Zachary Charles, Zheng Xu, Gauri Joshi, H. Brendan McMahan, Blaise Agüera y Arcas, Maruan Al-Shedivat, Galen Andrew, Salman Avestimehr, Katharine Daly, Deepesh Data, Suhas Diggavi, Hubert Eichner, Advait Gadhiar, Zachary Garrett, Antonious M. Girgis, Filip Hanzely, Andrew Hard, Chaoyang He, Samuel Horvath, Zhouyuan Huo, Alex Ingerman, Martin Jaggi, Tara Javidi, Peter Kairouz, Satyen Kale, Sai Praneeth Karimireddy, Jakub Konecny, Sanmi Koyejo, Tian Li, Luyang Liu, Mehryar Mohri, Hang Qi, Sashank J. Reddi, Peter Richtarik, Karan Singhal, Virginia Smith, Mahdi Soltanolkotabi, Weikang Song, Ananda Theertha Suresh, Sebastian U. Stich, Ameet Talwalkar, Hongyi Wang, Blake Woodworth, Shanshan Wu, Felix X. Yu, Honglin Yuan, Manzil Zaheer, Mi Zhang, Tong Zhang, Chunxiang Zheng, Chen Zhu, and Wenzhan Zhu. A Field Guide to Federated Optimization. *arXiv preprint arXiv:2107.06917*, 2021.
- [54] Kevin Hsieh, Amar Phanishayee, Onur Mutlu, and Phillip Gibbons. The Non-IID Data Quagmire of Decentralized Machine Learning. In *Proc. Int. Conf. on Machine Learning (ICML)*, Jul 2020.

- [55] Akhilan Boopathy and Ila Fiete. Gradient-trained Weights in Wide Neural Networks Align Layerwise to Error-scaled Input Correlations. *arXiv preprint arXiv:2106.08453*, 2021.
- [56] Joseph Mellor, Jack Turner, Amos Storkey, and Elliot Crowley. Neural Architecture Search without Training. In *Proc. Int. Conf. on Machine Learning (ICML)*, Jul 2021.
- [57] Jingzhao Zhang, Tianxing He, Suvrit Sra, and Ali Jadbabaie. Why gradient clipping accelerates training: A theoretical justification for adaptivity. In *Proc. Int. Conf. on Learning Representations (ICLR)*, 2020.
- [58] Xinlei Chen, Saining Xie, and Kaiming He. An Empirical Study of Training Self-Supervised Vision Transformers. In *Proc. Int. Conf. on Computer Vision (ICCV)*, 2021.
- [59] HuggingFace. Why is grad norm clipping done during training by default? <https://discuss.huggingface.co/t/why-is-grad-norm-clipping-done-during-training-by-default/1866>, 2020. Discussion forum.
- [60] Liyuan Liu, Xiaodong Liu, Jianfeng Gao, Weizhu Chen, and Jiawei Han. Understanding the Difficulty of Training Transformers. In *Proc. Conf. on Empirical Methods in Natural Language Processing (EMNLP)*, April 2020.
- [61] Yann Dauphin and Ekin Dogus Cubuk. Deconstructing the Regularization of BatchNorm. In *Proc. Int. Conf. on Learning Representations (ICLR)*, 2021.
- [62] Vitaliy Chiley, Ilya Sharapov, Atli Kosson, Urs Koster, Ryan Reece, Sofia Samaniego de la Fuente, Vishal Subbiah, and Michael James. Online Normalization for Training Neural Networks. In *Proc. Adv. in Neural Information Processing Systems (NeurIPS)*, 2019.

Appendix

The appendix is organized as follows:

- Appendix A: Details the setup for experiments conducted throughout the paper.
- Appendix B: Provides derivations for BatchNorm and GroupNorm gradients and elucidates similarity in their expressions.
- Appendix C: Completes the discussion of exploding/vanishing activations problem in the context of non-residual networks.
- Appendix D: Provides more results for the following experiments:
 - Section D.1: Train/Test curves for different configurations of *normalizer, model architecture, batch-size, and largest initial learning rate*.
 - Section D.2: Plots for Layer-wise cosine similarity at initialization for 10-layer non-residual network, 20-layer non-residual network, and ResNet-56 with different normalizers.
 - Section D.3: Plots for Gradient explosion at initialization for 10-layer non-residual networks, 20-layer non-residual network, and ResNet-56 with different normalizers and batch-sizes.

A Experimental Configurations

Our experiments are implemented using PyTorch and code is available at <https://github.com/EkdeepSLubana/BeyondBatchNorm>. Throughout the paper, we record several useful properties like variance of activations or gradient norm w.r.t. activations. For this purpose, we use PyTorch’s autograd library and define modules to calculate these properties without altering the input or gradients. Other experimental details are mentioned below.

Model Architectures: We focus on three model architectures: 10-layer non-residual networks, 20-layer non-residual networks, and ResNet-56. The non-residual networks architectures are detailed below. An integer X represents the number of filters in the layer; the tuple (X, y) represents the number of filters in the layer and the convolution’s stride respectively; the function $\text{block}(Z)$ represents a BasicBlock [24] used in ResNets, with X filters per layer and Z blocks. The final convolution layer’s output is average-pooled and fed into a linear-classifier.

1. 10-layer non-residual networks: [64, (64, 2), 128, (128, 2), 256, (256, 2), 512, (512, 2), 512, 512]
2. 20-layer non-residual networks: [64, 64, 64, (64, 2), 128, 128, 128, (128, 2), 256, 256, 256, (256, 2), 256, 256, 256, (256, 2), 512, 512, 512, 512]
3. ResNet-56: [32, $\text{block}(32, 9)$, $\text{block}(64, 9)$, $\text{block}(128, 9)$]

GroupNorm Configuration: An important architectural detail is the number of groups in GroupNorm. Following standard configurations in past work [3], we define number of groups at any layer to be 32. In experiments where group size, instead of number of groups was fixed, the number of groups at any given layer are determined by layer-width divided by group-size. This ensures the group size stays constant across all layers.

Batch-Sizes / Number of Training Epochs: We used batch-sizes of 256 and 16 in this work. Models with batch-size 256 are trained for 60 epochs, while models with batch-size 16 are trained for 10 epochs. Note that an epoch of training with batch-size 16 corresponds to $50000/16 = 3125$ training iterations, while an epoch of training with batch-size 256 corresponds to $50000/256 \approx 256$ training iterations. Hence, even though we use fewer number of training epochs for batch-size 16, the overall training budget for batch-size 16 is approximately 2.5 times the training budget for training at batch-size 256.

Learning Rates: The initial learning rates are equal to either 0.1 or 0.01. Following Goyal et al. [21], we linearly scale the learning rate when changing batch-size. At 80% training progress, we decay the learning rate by a factor of 10. For models trained in Figure 5, the initial learning rate was set to ensure most normalizers can train a model effectively. Thus, for non-residual networks with 10 layers and ResNet-56, we use initial learning rate of 0.1; for non-residual networks with 20 layers, we use initial learning rate of 0.01.

Other Hyperparameters: We train using SGD and use weight decay of 0.0001 with momentum of 0.9 for all models. Note that weight decay is known to have an interesting interplay with BatchNorm during training [12, 61], however we leave the study of these effects for other normalizers for future work.

Dataset / Preprocessing: For training models in Figure 1, Figure 4, and Figure 5, we use CIFAR-100 with random horizontal flipping while training, but no other data augmentation is applied. The samples are pre-processed to have a mean/std of 0.5 in all dimensions, following standard practice with CIFAR datasets.

Calculating Activations’ Variance/Cosine Similarity/Gradient Norm: In Figure 2, Figure 3, Figure 10, Figure 5, and Figure 8, we directly use CIFAR-100 samples without any augmentations for calculating the required properties. Samples are pre-processed to have a mean/std of 0.5 in all dimensions. We calculate the activations’ variance/cosine similarity/gradient norm using custom modules (defined using PyTorch’s autograd library) during forward/backward pass. All experiments use a batch-size of 256 and are averaged over 10 batches. For gradient explosion experiments using batch-size of 16, we average over 160 batches to match the number of samples used with batch-size 256.

Calculating Rank/Cosine Similarity in Figure 6a and Figure 6b: For calculating both rank and cosine similarity, we use random gaussian inputs. Via this, one can ensure the input has sufficiently distinct samples. Thus, if a normalizer results in high similarity of activations, that is an evident failure mode. This setup is in fact similar to Daneshmand et al. [4], who also use gaussian inputs for rank estimation. Following the authors, we use stable rank $\left(= \frac{\text{trace}(\Delta^T \Delta)}{\|\Delta\|_2^2}\right)$ for a matrix Δ for approximating rank in our experiments. This helps alleviate numerical precision problems, where relatively small magnitude singular values may end up contributing to the estimated rank.

B Gradient Derivations

We first redefine notations to focus on only the relevant variables. Specifically, we denote activations for a batch of N samples at layer L as $\mathbf{Y}_L \in \mathbb{R}^{D_L \times N}$, where D_L is the dimension of a given sample’s activations. The weight matrix is denoted as $\mathbf{W}_L \in \mathbb{R}^{D_{L-1} \times D_L}$. Two sets of outputs are relevant to us: (i) Pre-activations after weight multiplication, i.e., $\mathbf{X}_L = \mathbf{W}_L \mathbf{Y}_{L-1}$; (ii) Normalized pre-activations, i.e., $\hat{\mathbf{X}} = \mathcal{N}(\mathbf{X}_L)$, where \mathcal{N} denotes a normalizer. We will derive gradients for both BatchNorm and GroupNorm to show similarity between their expressions.

B.1 BatchNorm Gradients

Our derivation is similar to that of Chiley et al. [62], who also decompose the BatchNorm gradient into multiple projection operations. However, in that work, the authors focus on deriving an individual sample’s gradient only; meanwhile, we derive gradients for the entire batch. This is important because when using BatchNorm, the gradient of a sample is affected by activations of a different sample (i^{th} sample’s activations use j^{th} sample’s activations for calculating mean and variance in normalization). We define the BatchNorm operation as follows ²:

$$\begin{aligned} \hat{\mathbf{X}} &= \text{BN}(\mathbf{X}_L) \\ &= \sigma(\mathbf{X}_L)^{-1} (\mathbf{X}_L - \mu(\mathbf{X}_L)). \end{aligned} \tag{1}$$

Here, we define $\mu(\mathbf{X}_L) := (\frac{1}{N} \mathbf{X}_L \mathbf{1}) \mathbf{1}^T$ to perform mean-centering along the batch dimension and define $\sigma(\mathbf{X}_L) := \text{diag} \left((\mathbf{X}_L - (\frac{1}{N} \mathbf{X}_L \mathbf{1}) \mathbf{1}^T) (\mathbf{X}_L - (\frac{1}{N} \mathbf{X}_L \mathbf{1}) \mathbf{1}^T)^T \right)^{1/2}$ to perform the variance normalization operation. This method of defining BatchNorm is similar to that of Daneshmand et al. [4].

Note that the k^{th} diagonal element in matrix $\sigma(\mathbf{X}_L)$, denoted $\sigma(\mathbf{X}_L)^{(k)}$, is the variance along the batch-dimension for the k^{th} index across all samples’ pre-activations. We now calculate the derivative of this element with respect to the i^{th} sample’s pre-activations, i.e., $\mathbf{X}_{L,i}$. Since only the k^{th} element

²We ignore the affine scale and shift parameters (defined as γ, β in the main paper) as they are initialized to one and zero, respectively. That is, they do not influence our discussion in any way at initialization.

of $\mathbf{X}_{L,i}$, denoted $\mathbf{X}_{L,i}^{(k)}$, is of relevance to the variance calculation operation, we focus on it specifically. We use $\mu(\mathbf{X}_L)^{(k)}$ to index the mean matrix. This leads to the following:

$$\begin{aligned}\sigma(\mathbf{X}_L)^{(k)} &= \left(\frac{1}{N} \sum_n \left(\mathbf{X}_{L,n}^{(k)} - \mu(\mathbf{X}_L)^{(k)} \right)^2 \right)^{1/2} \\ \Rightarrow \frac{\partial}{\partial \mathbf{X}_{L,i}^{(k)}} \sigma(\mathbf{X}_L)^{(k)} &= \frac{1}{N \sigma(\mathbf{X}_L)^{(k)}} \sum_n \left(\left(\mathbf{X}_{L,n}^{(k)} - \mu(\mathbf{X}_L)^{(k)} \right) \left(\delta_{i,n} - \frac{1}{N} \right) \right) \\ &= \frac{1}{N \sigma(\mathbf{X}_L)^{(k)}} \left(\mathbf{X}_{L,i}^{(k)} - \mu(\mathbf{X}_L)^{(k)} \right) \\ &= \frac{1}{N} \hat{\mathbf{X}}_{L,i}^{(k)}\end{aligned}\quad (2)$$

where $\delta_{i,n} = 1$ if $i = n$ and 0 otherwise. A similar calculation can be conducted for the mean matrix too:

$$\mu(\mathbf{X}_L)^{(k)} = \frac{1}{N} \sum_n \left(\mathbf{X}_{L,n}^{(k)} \right) \Rightarrow \frac{\partial}{\partial \mathbf{X}_{L,i}^{(k)}} \mu(\mathbf{X}_L)^{(k)} = \frac{1}{N}. \quad (3)$$

Now, for the j^{th} sample's normalized pre-activations, we have the following:

$$\begin{aligned}\frac{\partial}{\partial \mathbf{X}_{L,i}^{(k)}} \hat{\mathbf{X}}_{L,j}^{(k)} &= \frac{\partial}{\partial \mathbf{X}_{L,i}^{(k)}} \left(\frac{\mathbf{X}_{L,j}^{(k)} - \mu(\mathbf{X}_L)^{(k)}}{\sigma(\mathbf{X}_L)^{(k)}} \right) \\ &= \frac{1}{(\sigma(\mathbf{X}_L)^{(k)})^2} \left[\sigma(\mathbf{X}_L)^{(k)} \left(\delta_{i,j} - \frac{\partial}{\partial \mathbf{X}_{L,i}^{(k)}} \mu(\mathbf{X}_L)^{(k)} \right) - \left(\mathbf{X}_{L,j}^{(k)} - \mu(\mathbf{X}_L)^{(k)} \right) \frac{\partial}{\partial \mathbf{X}_{L,i}^{(k)}} \sigma(\mathbf{X}_L)^{(k)} \right].\end{aligned}$$

We can use expressions derived in Equations 2 and 3 to complete the above equation as follows:

$$\frac{\partial}{\partial \mathbf{X}_{L,i}^{(k)}} \hat{\mathbf{X}}_{L,j}^{(k)} = \frac{1}{\sigma(\mathbf{X}_L)^{(k)}} \left(\left(\delta_{i,j} - \frac{1}{N} \right) - \frac{1}{N} \hat{\mathbf{X}}_{L,i}^{(k)} \hat{\mathbf{X}}_{L,j}^{(k)} \right). \quad (4)$$

We now calculate the gradient of loss (J) with respect to $\mathbf{X}_{L,i}^{(k)}$. Specifically, we use the relationship in Equation 4 to derive the following:

$$\begin{aligned}\frac{\partial}{\partial \mathbf{X}_{L,i}^{(k)}} (J) &= \sum_j \frac{\partial}{\partial \hat{\mathbf{X}}_{L,j}^{(k)}} (J) \frac{\partial}{\partial \mathbf{X}_{L,i}^{(k)}} \hat{\mathbf{X}}_{L,j}^{(k)} \\ &= \sum_j \frac{\partial}{\partial \hat{\mathbf{X}}_{L,j}^{(k)}} (J) \left(\frac{1}{\sigma(\mathbf{X}_L)^{(k)}} \left(\left(\delta_{i,j} - \frac{1}{N} \right) - \frac{1}{N} \hat{\mathbf{X}}_{L,i}^{(k)} \hat{\mathbf{X}}_{L,j}^{(k)} \right) \right) \\ &= \frac{1}{\sigma(\mathbf{X}_L)^{(k)}} \left(\frac{\partial}{\partial \hat{\mathbf{X}}_{L,i}^{(k)}} (J) - \frac{1}{N} \sum_j \frac{\partial}{\partial \hat{\mathbf{X}}_{L,j}^{(k)}} (J) - \frac{\hat{\mathbf{X}}_{L,i}^{(k)}}{N} \sum_j \hat{\mathbf{X}}_{L,j}^{(k)} \frac{\partial}{\partial \hat{\mathbf{X}}_{L,j}^{(k)}} (J) \right) \\ &= \frac{1}{\sigma(\mathbf{X}_L)^{(k)}} \left(\frac{\partial}{\partial \hat{\mathbf{X}}_{L,i}^{(k)}} (J) - \frac{1}{N} \nabla_{\hat{\mathbf{X}}_L} (J)^{(k)} \mathbf{1} - \frac{\hat{\mathbf{X}}_{L,i}^{(k)}}{N} \nabla_{\hat{\mathbf{X}}_L} (J)^{(k)} (\hat{\mathbf{X}}_L^{(k)})^T \right).\end{aligned}\quad (5)$$

Here, $\nabla_{\hat{\mathbf{X}}_L} (J)^{(k)}$ denotes the k^{th} row of the gradient of loss with respect to normalized pre-activations $\hat{\mathbf{X}}_L$. Similarly, $\hat{\mathbf{X}}_L^{(k)}$ denotes the k^{th} row of the normalized pre-activations matrix.

We can extend Equation 5 to the entire pre-activations matrix, as shown in the following:

$$\nabla_{\mathbf{X}_L} (J) = \sigma(\mathbf{X}_L)^{-1} \left(\nabla_{\hat{\mathbf{X}}_L} (J) - \frac{1}{N} \nabla_{\hat{\mathbf{X}}_L} (J) \mathbf{1} \mathbf{1}^T - \frac{1}{N} \text{diag} \left(\nabla_{\hat{\mathbf{X}}_L} (J) \hat{\mathbf{X}}_L^T \right) \hat{\mathbf{X}}_L \right). \quad (6)$$

Define the Oblique-manifold $\text{Ob}(\frac{1}{\sqrt{N}} \hat{\mathbf{X}}_L) := \frac{1}{N} \text{diag}(\hat{\mathbf{X}}_L \hat{\mathbf{X}}_L^T) = \text{diag}(\mathbf{1})$ and the projection operator $\mathcal{P}_{\text{Ob}(\frac{1}{\sqrt{N}} \hat{\mathbf{X}}_L)}^\perp[\mathbf{Z}] = \mathbf{Z} - \frac{1}{N} \text{diag}(\mathbf{Z} \hat{\mathbf{X}}_L^T) \hat{\mathbf{X}}_L$ that removes the component of Z inline with the normalized pre-activations. Similarly, define the projection operator related to the all-ones vector $\mathbf{1}$, which mean-centers its input along the batch-dimension: $\mathcal{P}_\perp^\perp[\mathbf{Z}] = \mathbf{Z} (I - \frac{1}{N} \mathbf{1} \mathbf{1}^T)$. Using these definitions along

with the fact the normalized pre-activations satisfy $\hat{\mathbf{X}}_L \mathbf{1} = \mathbf{0}$, we get:

$$\begin{aligned}\nabla_{\mathbf{X}_L}(J) &= \sigma(\mathbf{X}_L)^{-1} \left(\mathcal{P}_1^\perp \left[\mathcal{P}_{\text{Ob}(\frac{1}{\sqrt{N}} \hat{\mathbf{X}}_L)}^\perp \left[\nabla_{\hat{\mathbf{X}}_L}(J) \right] \right] \right) \\ &= \sigma(\mathbf{X}_L)^{-1} \left(\mathcal{P} \left[\nabla_{\hat{\mathbf{X}}_L}(J) \right] \right),\end{aligned}\tag{7}$$

where, we used an overall projection operation $\mathcal{P}[\cdot] = \mathcal{P}_1^\perp \left[\mathcal{P}_{\text{Ob}(\frac{1}{\sqrt{N}} \hat{\mathbf{X}}_L)}^\perp [\cdot] \right]$.

Now, recall $\mathbf{X}_L = \mathbf{W}_L \mathbf{Y}_{L-1}$. Thus, $\nabla_{\mathbf{Y}_{L-1}}(J) = \mathbf{W}_L^T \nabla_{\mathbf{X}_L}(J)$. We now redefine σ in the general way used in the main paper, i.e., $\sigma_{\{N\}}(\mathbf{X}_L)$, to denote the batch-variance operator that calculates variance along the batch-dimension $\{N\}$. Then, using Equation 7, we get our desired result:

$$\nabla_{\mathbf{Y}_{L-1}}(J) = \frac{1}{\sigma_{\{N\}}(\mathbf{X}_L)} \mathbf{W}_L^T \left(\mathcal{P} \left[\nabla_{\hat{\mathbf{X}}_L}(J) \right] \right),\tag{8}$$

as was shown in the main paper. This completes the derivation.

B.2 GroupNorm Gradients

We now derive gradients for GroupNorm. The derivation is quite similar to that of BatchNorm, but the definitions and order of operations changes substantially now. As we will see though, the final expression is essentially the same: a projection operation followed by a division by variance operation.

To begin, we first note that unlike BatchNorm, a given sample is normalized independently of other samples and hence we can analyze only a single sample for our discussion. We thus analyze activations $\mathbf{Y}_L \in \mathbb{R}^{D_L \times 1}$ for a single sample at layer L , distinguishing between pre-activations ($\mathbf{X}_L = \mathbf{W} \mathbf{Y}_{L-1}$) and normalized pre-activations ($\hat{\mathbf{X}}_L = \mathcal{N}(\mathbf{X}_L)$), as we did before in BatchNorm. We define the GroupNorm operation as follows³:

$$\begin{aligned}\hat{\mathbf{X}}^{(g)} &= \text{GN}(\mathbf{X}_L^{(g)}) \\ &= \frac{1}{\sigma_g} \left(\mathbf{X}_L^{(g)} - \mu_g \mathbf{1} \right).\end{aligned}\tag{9}$$

Here, we assume the activations \mathbf{X}_L have been divided into groups of size G and we use the notation $\mathbf{X}_L^{(g)}$ to denote the g^{th} group. The variable μ_g denotes the mean of the g^{th} group's activations and σ_g denotes the standard deviation. That is, $\mu_g = \frac{1}{G} \mathbf{X}_L^{(g)T} \mathbf{1}$, where $\mathbf{1}$ is an all-ones vector of dimension G . Similarly, $\sigma_g = \sqrt{\frac{1}{G} \sum_k \left(\mathbf{X}_{L,k}^{(g)} - \mu_g \right)^2}$, where, *in contrast with our discussion on BatchNorm, we use $X_{L,k}$ to index the neuron or channel in a given sample \mathbf{X}_L .*

With the notations established, we now begin the main derivation. We first calculate the partial derivative of the mean and standard deviation with respect to $\mathbf{X}_{L,i}^{(g)}$.

$$\begin{aligned}\sigma_g &= \left(\frac{1}{G} \sum_k \left(\mathbf{x}_{L,k}^{(g)} - \mu_g \right)^2 \right)^{1/2} \\ \implies \frac{\partial}{\partial \mathbf{X}_{L,i}^{(g)}} \sigma_g &= \frac{1}{G \sigma_g} \sum_k \left(\left(\mathbf{X}_{L,k}^{(g)} - \mu_g \right) \left(\delta_{i,k} - \frac{1}{G} \right) \right) \\ &= \frac{1}{G \sigma_g} \left(\mathbf{X}_{L,i}^{(g)} - \mu_g \right) \\ &= \frac{1}{G} \hat{\mathbf{X}}_{L,i}^{(g)}\end{aligned}\tag{10}$$

where $\delta_{i,n} = 1$ if $i = n$ and 0 otherwise. A similar calculation can be conducted for the mean matrix too:

$$\mu_g = \frac{1}{G} \sum_k \left(\mathbf{X}_{L,k}^{(g)} \right) \implies \frac{\partial}{\partial \mathbf{X}_{L,i}^{(g)}} \mu_g = \frac{1}{G}.\tag{11}$$

³We again ignore the affine scale and shift parameters (defined as γ, β in the main paper) as they are initialized to one and zero, respectively. That is, they do not influence our discussion in any way at initialization.

Since the i^{th} neuron (or channel) plays a role in the normalization of the j^{th} sample's pre-activations through mean/variance estimation operations, they will influence each other's gradients during the backward pass. Thus, we have the following:

$$\begin{aligned}
\frac{\partial}{\partial \mathbf{X}_{L,i}^{(g)}} \hat{\mathbf{X}}_{L,i}^{(g)} &= \frac{\partial}{\partial \mathbf{X}_{L,i}^{(g)}} \left(\frac{\mathbf{X}_{L,j}^{(g)} - \mu_g}{\sigma_g} \right) \\
&= \frac{1}{(\sigma_g)^2} \left[\sigma_g \left(\delta_{i,j} - \frac{\partial}{\partial \mathbf{X}_{L,i}^{(g)}} \mu_g \right) - (\mathbf{X}_{L,j}^{(g)} - \mu_g) \frac{\partial}{\partial \mathbf{X}_{L,i}^{(g)}} \sigma_g \right] \\
&= \frac{1}{(\sigma_g)^2} \left[\sigma_g \left(\delta_{i,j} - \frac{1}{G} \right) - (\mathbf{X}_{L,j}^{(g)} - \mu_g) \frac{1}{G} \hat{\mathbf{X}}_{L,i}^{(g)} \right] \\
&= \frac{1}{(\sigma_g)} \left[\left(\delta_{i,j} - \frac{1}{G} \right) - \frac{1}{G} \hat{\mathbf{X}}_{L,i}^{(g)} \hat{\mathbf{X}}_{L,j}^{(g)} \right],
\end{aligned} \tag{12}$$

where we used expressions derived in Equations 10 and 11 to arrive at the second-last equality. We now calculate the gradient of loss (J) with respect to $\mathbf{X}_{L,i}^{(k)}$. Specifically, we use the relationship in Equation 12 to derive the following:

$$\begin{aligned}
\frac{\partial}{\partial \mathbf{X}_{L,i}^{(g)}} (J) &= \sum_j \frac{\partial}{\partial \hat{\mathbf{X}}_{L,j}^{(g)}} (J) \frac{\partial}{\partial \mathbf{X}_{L,i}^{(g)}} \hat{\mathbf{X}}_{L,j}^{(g)} \\
&= \sum_j \frac{\partial}{\partial \hat{\mathbf{X}}_{L,j}^{(g)}} (J) \left(\frac{1}{\sigma_g} \left(\left(\delta_{i,j} - \frac{1}{G} \right) - \frac{1}{G} \hat{\mathbf{X}}_{L,i}^{(g)} \hat{\mathbf{X}}_{L,j}^{(g)} \right) \right) \\
&= \frac{1}{\sigma_g} \left(\frac{\partial}{\partial \hat{\mathbf{X}}_{L,i}^{(g)}} (J) - \frac{1}{G} \sum_j \frac{\partial}{\partial \hat{\mathbf{X}}_{L,j}^{(g)}} (J) - \frac{\hat{\mathbf{X}}_{L,i}^{(g)}}{G} \sum_j \hat{\mathbf{X}}_{L,j}^{(g)} \frac{\partial}{\partial \hat{\mathbf{X}}_{L,j}^{(g)}} (J) \right) \\
&= \frac{1}{\sigma_g} \left(\frac{\partial}{\partial \hat{\mathbf{X}}_{L,i}^{(g)}} (J) - \frac{1}{G} \mathbf{1}^T \nabla_{\hat{\mathbf{X}}_L^{(g)}} (J) - \frac{1}{G} \left(\hat{\mathbf{X}}_L^{(g)T} \nabla_{\hat{\mathbf{X}}_L^{(g)}} (J) \right) \hat{\mathbf{X}}_{L,i}^{(g)} \right).
\end{aligned} \tag{13}$$

Here, the vector $\nabla_{\hat{\mathbf{X}}_L^{(g)}} (J)$ denotes the gradient of the loss with respect to the g^{th} group of normalized pre-activations $\hat{\mathbf{X}}_L^{(g)}$. The above equation is with respect to an individual element of the pre-activations, so we now expand it to the entire group as follows:

$$\begin{aligned}
\nabla_{\mathbf{X}_L^{(g)}} (J) &= \frac{1}{\sigma_g} \left(\nabla_{\hat{\mathbf{X}}_L^{(g)}} (J) - \frac{1}{G} \left(\mathbf{1}^T \nabla_{\hat{\mathbf{X}}_L^{(g)}} (J) \right) \mathbf{1} - \frac{1}{G} \left(\hat{\mathbf{X}}_L^{(g)T} \nabla_{\hat{\mathbf{X}}_L^{(g)}} (J) \right) \hat{\mathbf{X}}_L^{(g)} \right) \\
&= \frac{1}{\sigma_g} \left(I - \frac{1}{G} \mathbf{1} \mathbf{1}^T \right) \left(I - \frac{1}{G} \hat{\mathbf{X}}_L^{(g)} \hat{\mathbf{X}}_L^{(g)T} \right) \nabla_{\hat{\mathbf{X}}_L^{(g)}} (J) \\
&= \frac{1}{\sigma_g} \mathcal{P}_1^\perp \left[\mathcal{P}_{\mathbb{S}(\hat{\mathbf{X}}_L^{(g)})}^\perp \left[\nabla_{\hat{\mathbf{X}}_L^{(g)}} (J) \right] \right] \\
&= \frac{1}{\sigma_g} \mathcal{P} \left[\nabla_{\hat{\mathbf{X}}_L^{(g)}} (J) \right].
\end{aligned} \tag{14}$$

In the above, we defined the projection operator $\mathcal{P}[\cdot]$ to compose two separate projection operators. Specifically, the operator $\mathcal{P}_1^\perp[\mathbf{Z}] = \left(I - \frac{1}{G} \mathbf{1} \mathbf{1}^T \right) \mathbf{Z}$, which is similar as defined before in BatchNorm's derivation, with the slight difference that uses right-hand matrix multiplication (the geometric interpretation remains the same, however). Meanwhile, the operator $\mathcal{P}_{\mathbb{S}(\hat{\mathbf{X}}_L^{(g)})}^\perp[\mathbf{Z}] = \left(I - \frac{1}{G} \hat{\mathbf{X}}_L^{(g)} \hat{\mathbf{X}}_L^{(g)T} \right) \mathbf{Z}$ removes the component of its input inline with the g^{th} group of activations for the given sample by projecting it onto the spherical manifold defined by $\mathbb{S}(\hat{\mathbf{X}}_L^{(g)})$. This is similar to the Oblique-manifold projector in BatchNorm; however, this operator focus on an individual sample only.

Now, recall $\mathbf{X}_L = \mathbf{W}_L \mathbf{Y}_{L-1}$. Thus, $\nabla_{\mathbf{Y}_{L-1}} (J) = \mathbf{W}_L^T \nabla_{\mathbf{X}_L} (J)$. We now redefine σ in the general way used in the main paper, i.e., $\sigma_{\{g\}}(\mathbf{X}_L)$, to denote the group-variance operator that calculates variance along the group-dimension $\{g\}$. Then, using Equation 14, we can complete the derivation:

$$\nabla_{\mathbf{Y}_{L-1}^{(g)}} (J) = \frac{1}{\sigma_{\{g\}}(\mathbf{X}_L)} \mathbf{W}_L^T \left(\mathcal{P} \left[\nabla_{\hat{\mathbf{X}}_L^{(g)}} (J) \right] \right). \tag{15}$$

Comparing the final gradient expression for GroupNorm (Equation 15) and BatchNorm (Equation 8), we can clearly see both GroupNorm’s and BatchNorm’s gradient essentially involve a projection operation, followed by matrix multiplication with the layer weights and division by standard deviation of the pre-activations. The primary difference lies in how the standard deviation is computed. For GroupNorm, we use a group’s standard deviation, which is bound to be small than a Batch’s standard deviation (as argued in Section 5 using the arithmetic-mean \geq harmonic-mean inequality). The results in Figure 8 provide empirical demonstration of this claim.

C Circumventing Exploding/Vanishing Activations in Non-Residual Networks

For the case of non-residual networks, the problem of growing/vanishing variance does not manifest generally. To understand this, note that activations-based normalizers act on a combination of the batch, the channel, or the spatial dimensions and rescale the variance (or norm) in those dimensions to 1, thus avoiding both exploding/vanishing activations. For parametric normalizers, as discussed in Section 3.2, properly designed corrections can ensure the signal variance is preserved during forward propagation. This implies, by design, all normalizers mentioned in Table 1 ensure that activations neither explode nor vanish in the case of non-residual networks. We empirically demonstrate this behavior in Figure 10 for a 20-layer CNN. Except for Scaled Weight Standardization [23], all methods ensure the variance neither grows nor vanishes, hence corroborating our argument. Indeed, for a 20-layer CNN, Scaled Weight Standardization is unable to train for most training configurations we tried (see Figure 12).

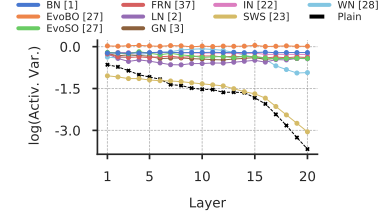


Figure 10: Log Activation Variance as a function of layer number in a 20 layer non-residual CNN. As shown, most normalization methods can avoid the problem of exploding/vanishing variance.

D More Results

D.1 Train/Test Curves for Different Configurations of Model Architecture, Normalizer, Batch-Size, and Initial Learning Rate

In the main paper, we provided training progress curves for a few configurations of model architecture, normalizer, batch-size, and initial learning rate. Here, we provide both train/test curves and several more settings. Specifically, Figure 11 contains results for non-residual CNNs with 10 layers; Figure 12 contains results for non-residual CNNs with 20 layers; Figure 13 contains results on ResNet-56 without SkipInit [6]; and Figure 14 contains results on ResNet-56 with SkipInit [6]. All results are averaged over 3 seeds and error bars show \pm standard deviation.

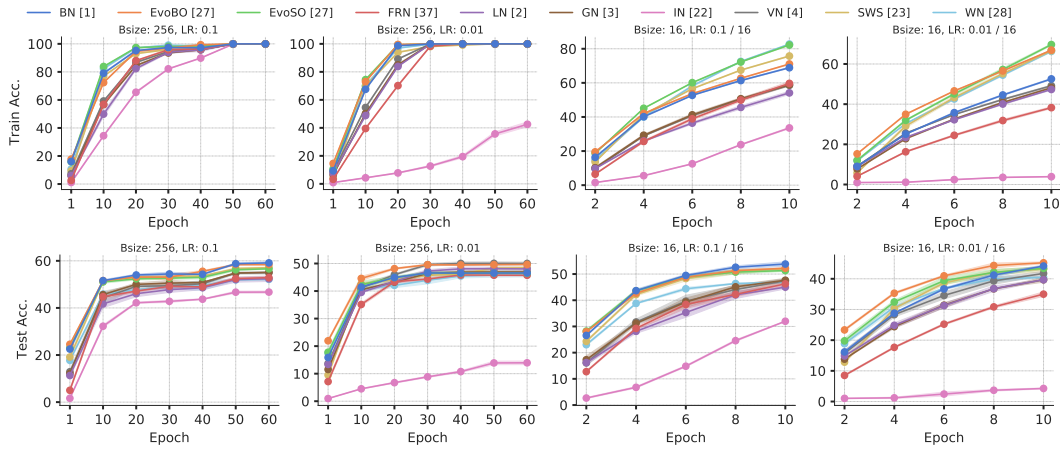


Figure 11: Non-Residual CNN with 10 layers

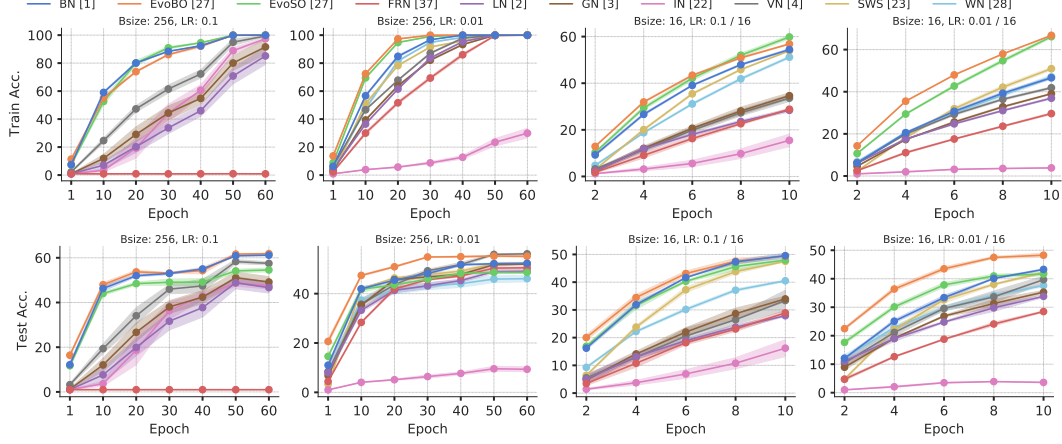


Figure 12: Non-Residual CNN with 20 layers

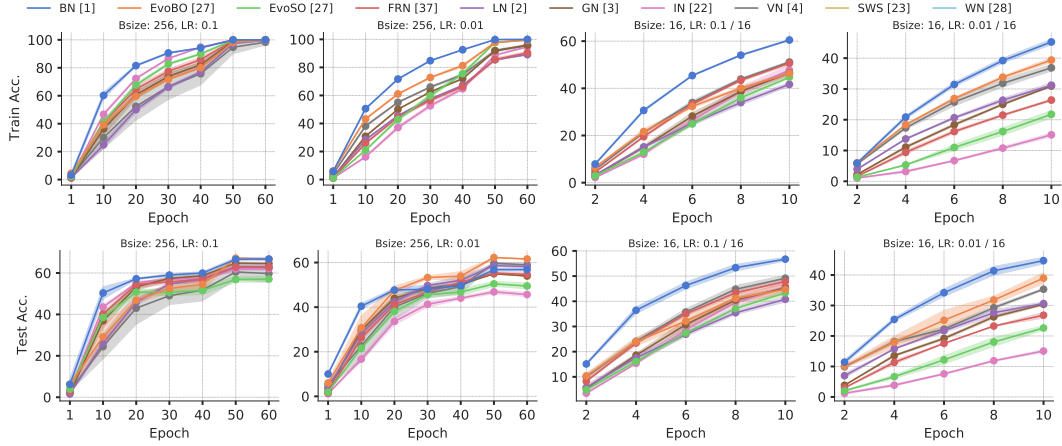


Figure 13: ResNet-56 without SkipInit

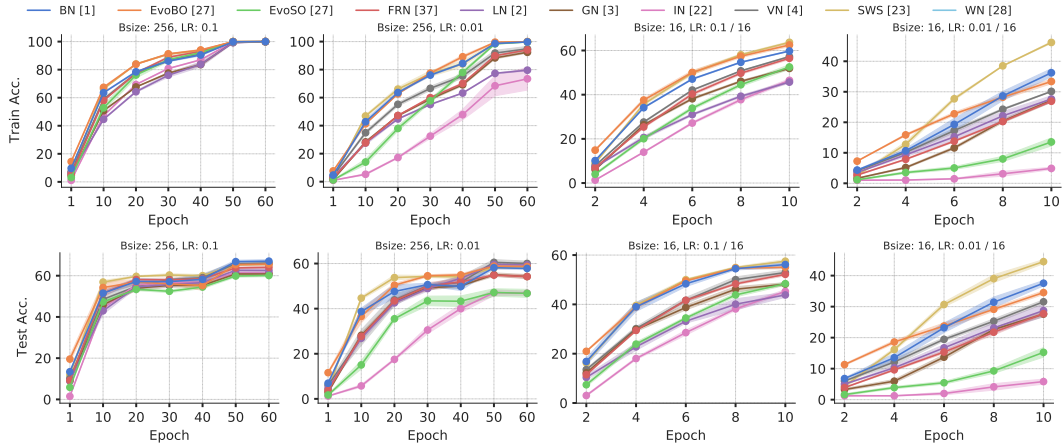


Figure 14: ResNet-56 with SkipInit

D.2 Cosine Similarity for Different Normalizers and Model Architecture Combinations

In the main paper, we discussed the implications of high similarity of activations for different input samples. Based on our discussion, we showed the tradeoff between group-size and cosine similarity

of activations in GroupNorm (and hence Instance Normalization/LayerNorm). However, it is worth noting that except for EvoNormSO [27], all normalizers use either batch variance or group variance for normalization. This indicates our discussion was general and hence applicable to all layers discussed in this paper. We show demonstration of this argument in Figure 15, where we find layers that rely on batch or group variance normalization have lower cosine similarity of activations.

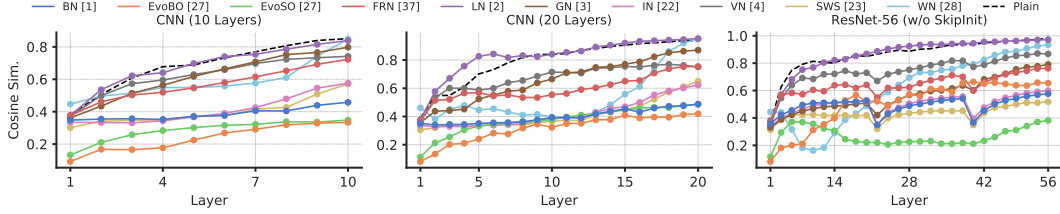


Figure 15: Cosine Similarity of activations for Non-Residual CNN with 10 layers, 20 layers, and ResNet-56 without SkipInit.

D.3 Gradient Explosion for Different Normalizers and Model Architecture Combinations

In Section 5, we discussed how gradient explosion instantiates in normalization layers which rely on batch-statistics or instance-statistics, while layers which use group-statistics can avoid this behavior. Here, we demonstrate our discussion holds generally true. For example, in Figure 16, we show gradient explosion is highest in Instance Normalization [22] and follows the order Instance Normalization \geq BatchNorm [1] \geq GroupNorm [3] \geq LayerNorm [2], as expected by our analysis, across several model architectures. Yang et al. [29] show ResNets are able to avoid gradient explosion by design. However, for the case of small batch-size (see Figure 17), we find gradient explosion continues to occur with Instance Normalization, even in ResNets. This again explains Instance Normalization’s inability to train effectively and stably.

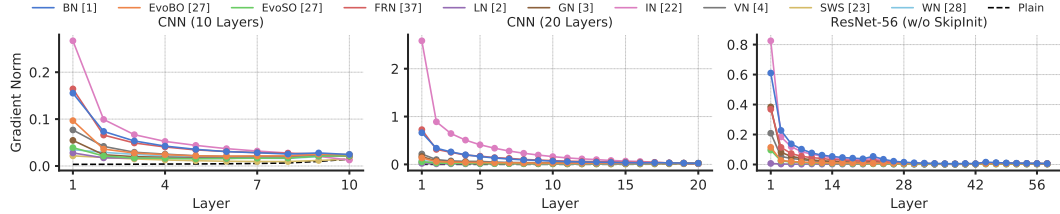


Figure 16: Batch-Size: 256

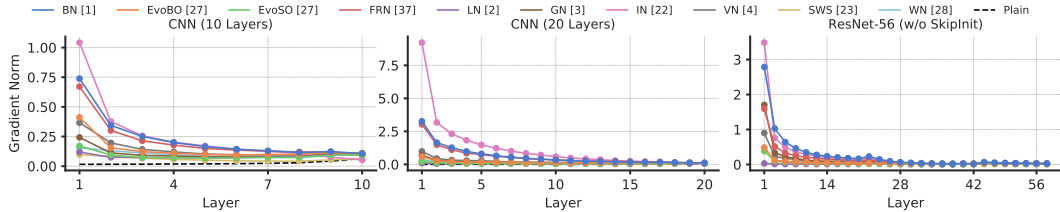


Figure 17: Batch-Size: 16